Novel Method for the Fabrication of Gradient-Index Plastic Optical Fibers

In-Sung Sohn and Chang-Won Park
Dept. of Chemical Engineering, University of Florida, Gainesville, FL 32611

A novel coextrusion method has been introduced for the fabrication of gradient-index plastic optical fibers (GI-POFs). In this method, the radial diffusion of a refractive-index-modifying dopant in a polymer matrix is enhanced significantly by a new die design concept. A theoretical analysis indicates that this new method can substantially reduce the material residence time required to obtain a smooth refractive-index profile, thereby increasing the output rate to a much higher level than possible with the conventional methods. An experiment using a poly(methyl methacrylate) (PMMA) with diphenyl sulfide (DPS) and diphenyl sulfoxide (DPSO) as the refractive-index-modifying dopants has shown an excellent agreement with the theoretical prediction, suggesting that the new coextrusion method is a viable way to manufacture a GI-POF with the bandwidth higher than 700 Mbits/s at a distance of 100 m.

Introduction

With the fast advancement of microelectronics technology, gradient-index plastic optical fibers (GI-POFs) have drawn much interest as high-speed data-transmission media for short-haul applications such as local area networks (LANs) and home networks. While the metal cables currently in use for most LANs are suitable for a data transmission rate of up to about 150 Mbits/s at a distance of 100 m (or 150 Mbps-100 m), new standards demand a much higher bandwidth, near 1 Gbps-100 m. Although such a high bandwidth cannot be met by the metal cables, it can be achieved by single-mode glass optical fibers (GOFs), which are made of high-quality silica glass. However, single-mode GOFs are as thin as $5 \sim 10$ μm in diameter, making them extremely fragile and difficult to be spliced (Senior, 1985). Thus, their use in LANs or home networks, where cables should be installed along curved paths and frequent connections should be made, is not practical.

GI-POFs have been recognized as a viable substitute for short-distance applications. Flexibility and durability of polymeric materials allow POFs to be large in diameter (on the order of 1 mm), although the special property of gradient-index profile is required to achieve the high bandwidth capability. Gradient-index profile refers to a refractive-index profile that varies continuously in the radial direction, as described in Figure 1. The most prevalent and simple type of optical fiber is the step-index (SI) fiber that has a core-cladding structure with a step change in the refractive-index profile. The bandwidth of SI-POFs is limited to about 150 Mbps-100 m due to the modal dispersion of input signals. The dispersion represents the broadening of the optical impulse as it propagates through the fiber. In geometrical optics, the modal dispersion is attributed to different paths followed by different rays that consist of the impulse input signal. The ray propagating along the fiber axis has the shortest path, whereas the path is longer for oblique rays. Consequently, different rays with different paths arrive at the output end of the fiber at different times, resulting in the broadening of the impulse input signal. This dispersion can be reduced if the speed of the rays can be adjusted in a way that the ray with a longer path travels at a higher average speed. Because the speed of light is inversely proportional to the refractive index of the medium, the gradient-index profile of GI-POFs reduces the modal dispersion, enabling high bandwidth data transmission. Especially when the refractive-index profile of GI-POFs is optimized to a near-parabolic shape, the modal dispersion is minimized, resulting in a bandwidth higher than 1 Gbps-100 m (Halley, 1987).

Due to the aforementioned advantages of GI-POFs, there have been numerous research efforts to develop various techniques for fabricating GI-POFs with an optimum refractive-

Correspondence concerning this article should be addressed to C.-W. Park.

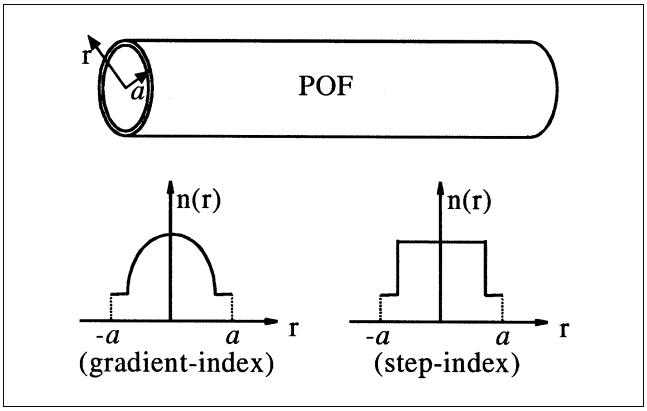

Figure 1. Step-index (SI) and a gradient-index (GI) plastic optical fiber.

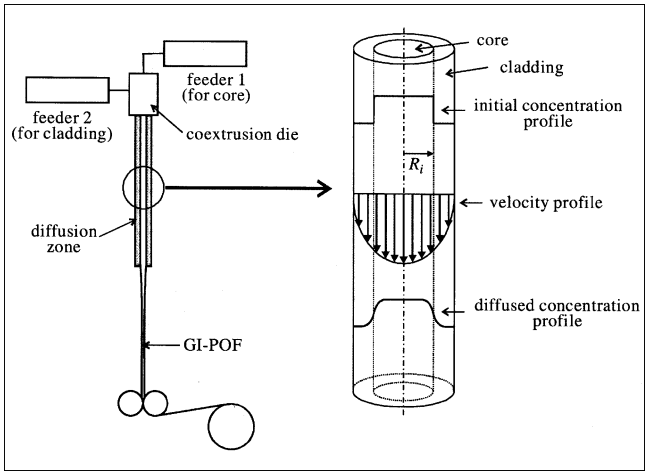

Figure 2. Diffusion-assisted coextrusion process.

index profile. The best-known method may be the *interfacial gel polymerization* that was introduced by Koike (1991) and further improved over the years by his coworkers (Koike et al., 1995; Ishigure et al., 1995, 1996, 1998). In this method, a transparent polymeric tube [such as polymethyl methacrylate (PMMA)] is prepared first. This tube is then filled with a mixture of a monomer and a nonreacting dopant (such as methyl methacrylate and benzyl benzoate) that is polymerized thermally while the cylindrical tube rotates about its axis. The inner wall of the tube is swollen by the monomer forming a thin gel phase. Due to the *gel effect*, the polymerization reaction is faster in the gel phase than in the monomer bulk phase. Consequently, the reaction occurs preferentially on the inner surface of the tube, and the polymer phase grows inward toward the center of the tube as the reaction progresses. Since the molecular volume of the dopant is typically larger than that of the monomer, the monomer diffuses into the gel phase faster and reacts. Consequently, the dopant is rejected from the polymerization site, and its concentration becomes gradually higher toward the center of the cylinder as the polymerization reaction progresses. Thus, a concentration gradient of the dopant is created in the radial direction. Once the polymerization reaction is complete, a rodlike cylindrical object called *preform* is made. Since the dopant increases the refractive index when dispersed in the polymer matrix, the preform made by this method has a gradually increasing refractive index toward the center. The preform is then heat-drawn to a GI-POF. Other methods include the *copolymerization in a centrifugal field* by van Duijnhoven and Bastiaansen (1999), and coextrusion methods (Ho et al., 1995; Liu et al., 1999a,b; Park et al., 2000).

Another method called the *diffusion-assisted coextrusion process* was introduced recently by Sohn and Park (2001, 2002). In this process, two polymers for core and cladding, respectively, are fed into a coextrusion die by two separate feeders where a concentric core-cladding structure is formed (Figure 2). The core material contains a refractive-index-modifying additive that diffuses from the core into the cladding polymer in the diffusion zone. The diffusion zone is a cylindrical tube of a finite length that is heated from outside to maintain the material in a molten state at a desired temperature. Once the material with the core-cladding structure leaves the diffusion zone, it is stretched to a desired radius and solidified by cooling. Since the material is solidified in a nonequilibrium state, a continuously varying additive concentration profile (hence, the -index profile) is created in the radial direction (Figure 2). It has been shown that the refractive-index profile created by the diffusion-assisted coextrusion process can provide a bandwidth substantially higher than that obtainable with a step-index profile. However, a rather long residence time is required in the diffusion zone in order to induce a substantial change in the refractive-index profile by the diffusion process. This long-residence-time requirement is not just for the *diffusion-assisted coextrusion process*, but for all coextrusion processes in which the refractive-index profile is altered by slow molecular diffusion. It is a serious deficiency of the coextrusion processes, because a long residence time can result in degradation of polymers and consequent contamination that deteriorates the optical property of the GI-POF.

In this article, a novel method for overcoming the deficiency of the conventional coextrusion processes is suggested. A theoretical analysis, confirmed by experiment, indicates that a refractive-index profile close to the optimum parabolic shape can be obtained with a much shorter residence time than required by the conventional methods. In the following section, the new method is described, followed by a theoretical analysis for the convective diffusion of an additive in a polymer melt. Experimental confirmation of the theoretical predictions is then described. The ray analysis is also described briefly for the bandwidth estimation for a given refractive-index profile. Finally, a summary and conclusion is given.

Convective Diffusion in a Novel Coextrusion Die

The new method for the enhanced diffusion of an additive from the core material to the cladding relies on the novel design of a coextrusion die that is shown in Figure 3. The new die consists of a feeding zone, a diffusion zone, and a converging zone. The novel feature of this design is the presence of the inner mandrel that creates the diffusion zone of an annulus shape and the subsequent converging zone. The

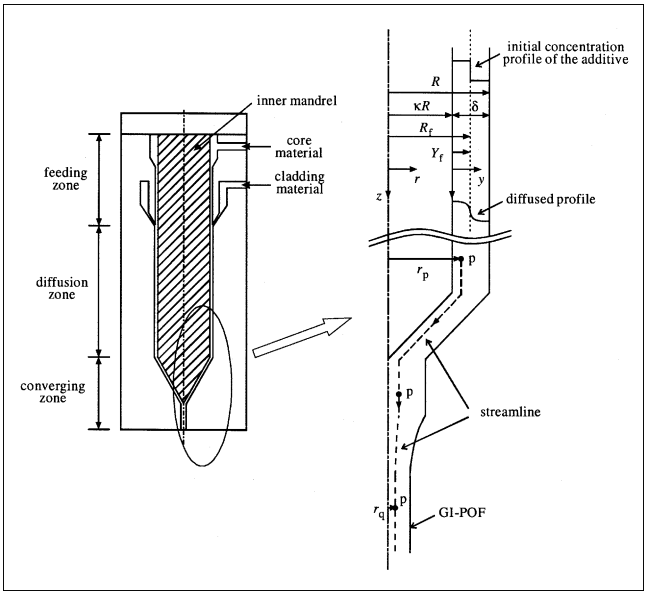

Figure 3. Annulus die for the new coextrusion process.

annular geometry of the diffusion zone makes the contact area between the core and the cladding materials much larger than that in the conventional coextrusion dies, thereby increasing the total diffusion rate of the additive in the radial direction by an order of magnitude. Once the diffusion is achieved to a significant level, the core and cladding materials in the annular structure are reshaped into a concentric cylindrical form in the converging zone, and it is then drawn into a fiber.

While the overall process of fiber formation involves different types of flows in each region in Figure 3, the main interest of the present article is in the convective diffusion occurring in the annular diffusion zone as compared with that in the cylindrical diffusion zone described in Figure 2. The radial diffusion of an additive that occurs in the diffusion zone from the core to the cladding material can be described by the following steady convective diffusion equation

$$\boldsymbol{u}\cdot\nabla\tilde{c}(r,\tilde{z}) = D\nabla^2\tilde{c}(r,\tilde{z}) \tag{1}$$

Here $\boldsymbol{u}$ is the velocity vector in the annulus geometry; $\tilde{c}$ is the additive concentration that depends on the radial and the axial coordinates, as described in Figure 3; and D is the diffusivity of the additive. The boundary conditions include the no-flux condition at the inner ($r = \kappa R$) and outer solid walls ($r = R$) and the initial concentration profile at $\tilde{z} = 0$

$$\text{at} \quad r = \kappa R \text{ and } R, \qquad \frac{\partial\tilde{c}}{\partial r} = 0 \tag{2a, 2b}$$

$$\text{at} \quad \tilde{z} = 0, \qquad \begin{cases} \tilde{c} = \tilde{c}_o & \text{for} \quad \kappa R < r < R_f \\ \tilde{c} = 0 & \text{for} \quad R_f < r < R, \end{cases} \tag{3}$$

where R_f is the location of the interface between the core and the cladding, which is known once the flow rates of the core and cladding materials are specified, and $\tilde{z} = 0$ represents the inlet to the diffusion zone where the flow field is assumed axisymmetric and fully developed. The initial condition described by Eq. 3 is equivalent to the case in which the core material contains an additive at a uniform concentration of $\tilde{c}_o$, whereas the cladding is a pure polymer melt. This initial condition has been chosen in accordance with the experimental condition that will be described in the following section.

In order to make analytic progress, it is further assumed that the core and the cladding materials are Newtonian fluids with the same viscosity. The polymer melts are certainly not Newtonian. However, their shear-thinning behavior is not significant when the shear rate is very low, as is the case for the flow in the annular diffusion zone. Thus, the Newtonian assumption is not necessarily a serious drawback of the present analysis. As also will be described later, the shear rate in the coextrusion die under our experimental conditions is smaller than 10 s^{-1}, and the power-law index of the polymer in that shear rate range is greater than 0.8, indicating weak shear-thinning behavior. Furthermore, the analytic result obtained under the Newtonian assumption matches very closely with that of numerical calculation in which the shear-thinning behavior of the polymer has been taken into account by adopting the power-law fluid model. The presence of an additive in the core material may have an influence on its rheological properties. For simplicity, however, it also has been assumed that the changes in the rheological properties are negligible.

Under the prescribed assumptions, the axial component of the velocity in Eq. 1 is given as

$$u_z = \frac{\Delta pR^2}{4\mu L}\left[1-\left(\frac{r}{R}\right)^2+\left(\frac{1-\kappa^2}{\ln(1/\kappa)}\right)\ln\left(\frac{r}{R}\right)\right] \tag{4}$$

Although the velocity field is given in an analytic form, it is complicated enough not to allow an analytic solution for the concentration profile. However, further geometric simplification is possible, because the gap of the annulus (δ) is much smaller than its inner or outer radius (that is, $\delta \ll R$ or κR in Figure 3). When the origin of the coordinate system is moved to the inner surface of the annular gap and the variables are scaled as

$$y = \frac{r-\kappa R}{\delta} \qquad z = \frac{\tilde{z}}{L} \qquad c = \frac{\tilde{c}}{\tilde{c}_o},$$

Eq. 1 is reduced to

$$\frac{3}{\epsilon^2}\left[1-(1-\epsilon+\epsilon y)^2+\left(\frac{1-(1-\epsilon)^2}{\ln(1/(1-\epsilon))}\right)\ln(1-\epsilon+\epsilon y)\right]\frac{\partial c}{\partial z}$$
$$= k^2\left(\frac{\partial^2 c}{\partial y^2}+\frac{\epsilon}{1-\epsilon+\epsilon y}\frac{\partial c}{\partial y}+\epsilon^2\left(\frac{R}{L}\right)^2\frac{\partial^2 c}{\partial z^2}\right) \tag{5}$$

The scaling for the axial coordinate, L, is the length of the diffusion zone and the dimensionless parameters ϵ and k^2

are δ/R and $1/(\epsilon^2 Pe)$, respectively. Here Pe is the Peclet number defined as UL/D, where U is the average velocity of the material in the diffusion zone.

Because ϵ is a small parameter, the method of perturbation expansion can be applied to obtain a series solution for the dimensionless concentration profile, c, as follows

$$c = c^{(0)} + \epsilon c^{(1)} + \epsilon^2 c^{(2)} + \cdots \tag{6}$$

By substituting the expansion (Eq. 6) into Eq. 5 and linearizing it about ϵ and setting $\epsilon = 0$, the leading-order equation can be obtained as

$$6y(1-y)\frac{\partial c^{(0)}}{\partial z} = k^2 \frac{\partial^2 c^{(0)}}{\partial y^2} \tag{7}$$

In the same way, the leading-order boundary conditions are determined to be

$$\frac{\partial c^{(0)}}{\partial y} = 0 \qquad \text{at} \quad y = 0 \quad \text{and} \quad 1 \tag{8a, 8b}$$

$$c^{(0)}(y,0) = \begin{cases} 1 & \text{for} \quad 0 < y < Y_f \\ 0 & \text{for} \quad Y_f < y < 1 \end{cases} \tag{9}$$

Here Y_f is the position of the interface position in the y coordinate (that is, $Y_f = (R_f - \kappa R)/\delta$). Once the flow rates of the core and cladding materials are specified, Y_f is determined accordingly.

In deriving the leading-order equation, the axial diffusion term in the governing equation (Eq. 5) has been dropped because it is a small $O(\epsilon^2)$ term. Consequently, an elliptic equation has been changed to a parabolic one, and the perturbation expansion is singular. However, the perturbation expansion can be treated as if it is regular up to $O(\epsilon^2)$ by assuming that the amount of the additive is constant at every axial position. This assumption is plausible because the diffusion of the additive in the axial direction is, in fact, very small for the present problem for which the Peclet number is large.

Equations 7–9 represent the flow situation in a gap between two flat parallel plates where the curvature effect in the azimuthal direction in Figure 3 is neglected. Although not exactly the same, this set of equations is reminiscent of the classic Graetz problem for the convective heat transfer in a circular tube (Jakob, 1962; Siegel et al., 1958). Following the similar procedure as Graetz or our previous work (Sohn and Park, 2001), the solution to Eq. 7 satisfying the boundary conditions Eqs. 8 and 9 is determined to be

$$c^{(0)} = Y_f^2(3 - 2Y_f) + \sum_{n=1}^{\infty} \frac{2}{\beta_n} \frac{\left(\frac{dF_n}{dy}\right)_{y=Y_f}}{\left[F_n \frac{\partial}{\partial y}\left(\frac{\partial F_n}{\partial \beta_n}\right)\right]_{y=1}} e^{-\beta_n^2 k^2 z/6} F_n(y,\beta). \tag{10}$$

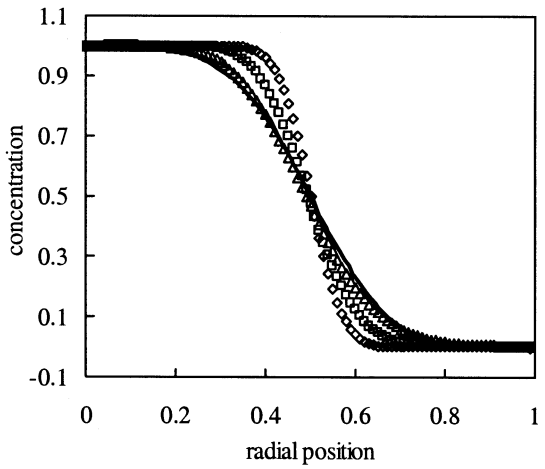

Figure 4. Additive concentration profiles in a GI-POF ($D = 10^{-6}$ cm^2/s, Q = 100 g/h).

Solid line is for the annulus diffusion zone with ID = 2.54 cm, δ = 0.159 cm, and length = 6.35 cm: symbols are for the tubular diffusion zone with ID = 0.384 cm and length = 18.4 cm (◇), 50 cm (□) or 100 cm (△).

Here F_n is the eigenfunction corresponding to the eigenvalue β_n. Interested readers will find the detailed solution procedure in the Appendix.

Equation 10 represents the leading-order approximation for the concentration profile in the annular diffusion zone. Yet, the profile of practical interest is the one for a cylindrical structure at the outlet from the converging zone in Figure 3. Assuming that the diffusion in the converging zone is negligible, the concentration profile at the end of the converging zone, and subsequently in the fiber, can be obtained by the material-balance equation. The fluid particle, p, at the radial position r_p in the diffusion zone flows downward following a streamline, and is located at a radial position, r_q, in the fiber, as depicted in Figure 3. Because the flow is laminar, the material balance requires the following relationship:

$$\int_{\kappa R}^{r_p} 2\pi r u_z \, dr = \pi r_q^2 U_f, \tag{11}$$

where u_z is the axial velocity in the diffusion zone given in Eq. 4, and U_f is the average velocity of the fiber; this is the total flow rate divided by the cross-sectional area of the fiber, because the flow quickly becomes a plug flow once the material leaves the converging zone. Thus, for a radial position in the diffusion zone, the corresponding radial position in the fiber is determined by Eq. 11.

In Figure 4, the additive concentration profile obtained with the annular-shaped die is compared to those obtained with the tubular-shaped one. The solid line represents the result for the annular-shaped die with an inner diameter of 2.54 cm, annulus gap of 0.159 cm, and length of 6.35 cm, whereas the symbols are for the tubular-shaped die, which has a tube diameter of 0.384 cm and lengths of 18.4 cm, 50 cm, and 100 cm, respectively. The diffusivity of the additive was set to be 10^{-6} cm^2/s, and the position of the interface was 0.331 for the annular-shaped die ($Y_f = 0.331$) and 0.366 for the tubular-shaped one (R_i = 0.366). The interfacial po-

sition of 0.331 in the annular zone (that is, $Y_f = 0.331$) is equivalent to that of 0.366 in the converging zone (that is, $R_i = 0.366$), and it becomes 0.5 in the cylindrical fiber that is drawn from the end of the converging zone. The total flow rate was set to be 100 g/h for all cases. The residence time in the annular diffusion zone was 6.1 min at the given output rate, and that in the tubular diffusion zone was 6.1, 16.5, and 33 min when the tube length was 18.4, 50, and 100 cm, respectively. The value of the additive diffusivity (10^{-6} cm^2/s) is based on our previous work, wherein we estimated its magnitude and the temperature dependence (Sohn and Park, 2002).

Additive concentrations obtained with the annular-shaped die show a much broader profile despite the short average residence time in the diffusion zone compared to those obtained with the tubular-shaped die. The results indicate that the average residence time required for the tubular-shaped die to obtain a profile close to that for the annular-shaped one at the same temperature and output is about six times longer. Consequently, the diffusion zone of the tubular geometry should be much longer than the length of the annular diffusion zone (18 times longer for the present case). The total diffusion rate of the additive in the radial direction is proportional to the contact area between the core and the cladding materials. Thus, the significant enhancement in the diffusion rate with the annular geometry is mainly due to the large increase in the contact area resulting from the presence of the inner mandrel.

The analytic solution given by Eq. 10 is for the leading order in ϵ, and has an error of $O(\epsilon)$, where ϵ is the ratio of the annulus gap to the outer radius (that is, $\epsilon = \delta/R$). The value of ϵ for the prescribed dimension of the annular diffusion zone for the result in Figure 4 is rather large, as 0.125, and higher-order solutions described in Eq. 6 may have to be considered in order to obtain a more accurate solution for the concentration profile. Instead of pursuing higher-order solutions, a numerical solution to the original equations without approximations (that is, Eqs. 1–3) has been determined using a finite-element method. In Figure 5, the numerical solution is compared to the leading-order analytic solution. The difference between them appears to be very small, suggesting that the leading-order solution is a reliable estimate for the additive concentration profile despite the fact that the value of ϵ is rather large.

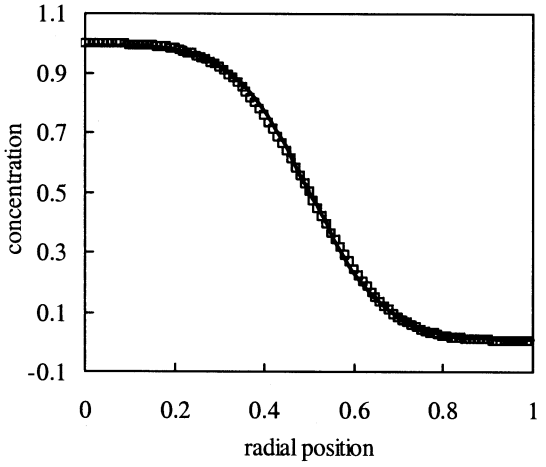

Figure 5. Comparison of the analytic solution for the leading order in ϵ and the numerical solution to the full governing equation (Eq. 1) for the additive concentration profile.

Open square is the analytic solution, $c^{(0)}$, and the solid line is for the numerical solution. $D = 10^{-6}$ cm^2/s, and the annulus dimension is the same as the one for Figure 4.

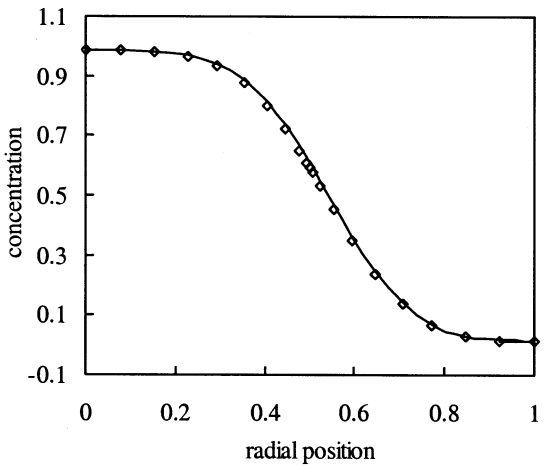

Figure 6. Additive concentration profile when the fluid is a Newtonian (solid line) or power-law fluid (open symbol).

As stated previously, the material has been assumed to be Newtonian in determining the leading-order solution, Eq. 10. In order to check whether the Newtonian assumption is a serious deficiency of the present analysis, another numerical solution to the full equations has been sought by assuming the material to be a power-law fluid. In Figure 6, the numerical solution for a power-law index of 0.8 is compared with the analytic solution with the Newtonian assumption. This particular value of the power-law index was chosen because the material that was used for the experiment (PMMA, provided by Cyro Industries) can be closely represented by the power-law model with a power-law index of 0.8 for the shear rate range between 0.1 and 10 s^{-1}. As was pointed out previously, the shear-thinning behavior of the material is not significant at the low shear rate, and results in a negligible difference in the concentration profile. These results suggest that the leading-order approximation presented in this section provides a reliable estimate for the additive concentration profile with a reasonable accuracy, justifying the simplifying assumptions described at the beginning of the section.

Experiment

An experimental study was conducted to compare the results with the predictions of the theoretical analysis described in the previous section. A PMMA obtained from Cyro Industries (Acrylite H-15) was used for both core and cladding, and a refractive-index-modifying additive was added to the core material in the form of a master batch (PMMA pellets containing the additive at a high concentration). Two different kinds of additives have been used for the present study:

(1) diphenyl sulfide (DPS), and (2) diphenyl sulfoxide (DPSO). The molecular weight and refractive index of DPS are 186 and 1.633, respectively, while those of DPSO are 202 and 1.606. These additives are known to have good compatibility with PMMA, and have a relatively high diffusivity at a processing temperature close to 200°C. Because the refractive index of both additives is much larger than that of PMMA, only a small amount is needed to induce a change in the refractive index. It is desirable to keep the additive concentration as low as possible, because it acts not only as a plasticizer that decreases the maximum service temperature of the GI-POF, but also as a source of light scattering that increases the attenuation of the fiber.

DPS and DPSO are also known to have good thermal stability at an elevated temperature. The thermal stability of GI-POF is important, because the refractive-index profile created by the additive concentration profile should not change when subjected to an elevated service temperature. Sato and coworkers (2000) have suggested that the thermal stability of the refractive-index profile is affected by the diffusivity and the plasticization effect of the additive, and the materials with polar groups attached to aromatic rings are most appropriate as the refractive-index-modifying additive. In their study, a GI-POF prepared by the interfacial gel polymerization method using PMMA, with DPS or DPSO as the dopant, did not show a detectable change in the refractive-index profile nor in the bandwidth characteristics after 12,000 h of aging at 85°C.

In order to ensure good dispersion of the additives in PMMA for the core, master batches (that is, PMMA chips or pellets containing the additives at high concentrations) were first prepared by dissolving both PMMA and DPS or DPSO in toluene and mixing them for 3 h. The mixture was then cast into a sheet and dried in a vacuum oven for 7 days. The dried plaque or sheet was broken into small chips of about 3 mm in its characteristic size. The additive concentration in the master batch was 20 wt %. For the core material, the master batch was dry-blended with pure PMMA pellets, making the final concentration 6.5 wt % for DPS-doped material and 7.5 wt % for a DPSO-doped one. Pure PMMA without any additive was used for the cladding.

The core and the cladding materials were extruded separately using two 19-mm extruders. Since PMMA is hygroscopic and therefore capable of absorbing moisture up to 0.3 wt % at room temperature, the materials were dried under vacuum at 70°C for at least 24 h prior to the extrusion. Otherwise, the absorbed moisture could generate numerous bubbles during extrusion. The total extrusion output was varied between 93 and 245 g/h to vary the residence time of the material in the diffusion zone, and the melt temperature was set within the range of 193 and 211°C.

A coextrusion die with the annular diffusion zone was designed with the idea of producing an additive concentration profile that is close to a parabolic shape in the central region of the fiber in addition to the typical requirement that the pressure drop in the die be greater than about 7,000 kPa at the given output in order to ensure a uniform flow rate around the circumference of the annulus region (Michaeli, 1991). The annulus dimension satisfying these design criteria was an inner diameter of 2.54 cm, a gap of 0.159 cm, and a length of 6.35 cm.

The core and the cladding materials are formed into a concentric structure in the coextrusion die, and the additive diffusion takes place at the core–cladding interface in the annular diffusion zone, forming a concentration gradient in the radial direction as described in Figure 3. The annular-shaped material is then turned into a cylindrical shape in the converging zone and is drawn into a fiber as it leaves the die exit. Although the typical diameter of a POF is between 0.5 and 1.0 mm, the fiber was set to be 3 mm in the present study to make the measurement of the concentration profile easier.

The additive-concentration profile in the fiber (hence, the refractive-index profile) was measured using an FT-IR spectrophotometer mounted with an optical microscope (Nicolet Magna FT-IR 760). The sample preparation and the measurement procedures were as follows. Thin disks of about 1 mm in thickness were cut from the 3-mm fiber using a wire saw. The disks were then ground to 100-μm-thick circular films using 400- and 2,000-grit abrasive papers followed by polishing using an aluminum oxide slurry (20 wt % aqueous solution of 50 nm Al_2O_3 at pH 4). The polishing procedure was necessary to eliminate the fine scratches on the film surface made by the abrasive papers. The circular film samples were then washed with deionized water and dried in a vacuum. The 100-μm-thick sample was then placed on a gold mirror under a microscope attached to the spectrometer, and light from a Nernst glower that was focused through a 10× object lens was lit on the sample. The light signal from the sample to the MCT detector includes reflected rays from the sample surface and from the gold mirror after passing through the sample. One hundred twenty-eight spectra within a spectral range of 1,400–2,000 cm^{-1} were collected and averaged for each point on the sample. This procedure was repeated while scanning the 3-mm-diam sample in the radial direction at a 50-μm interval. Thus, the spatial resolution of the additive concentration profile in the radial direction was 50 μm with 30 data points across the radius.

The additive concentration at each radial position in the sample is determined by the Beer's law, which provides a linear relationship between the signal intensity and the additive concentration (Ingle and Crouch, 1998)

$$A \equiv \log(I_0/I) = abc \tag{12}$$

Here A is the absorbance defined as the logarithm of the ratio of the incident to the transmitted light intensities. The terms a, b, and c are the absorptivity or extinction coefficient, the path length of the sample, and the concentration of the additive in grams per liter, respectively.

Results and Discussion

FT-IR spectra at three different radial positions of the DPS- and DPSO-doped fiber samples are shown in Figure 7. The peak appearing at 1,581 cm^{-1} is due to the phenyl group of either the DPS or DPSO molecule, and that at 1,749 cm^{-1} is due to the ester group of the PMMA molecule. The peak height at 1,581 cm^{-1}, which is largest at the center of the sample (that is, at $r = 0$), decreases with increasing radial position, whereas the ester peak at 1,749 cm^{-1} shows little variation with the radial position. The peak height (that is, the signal intensity) at 1,581 cm^{-1} is proportional to the additive concentration at the given radial position, according to the

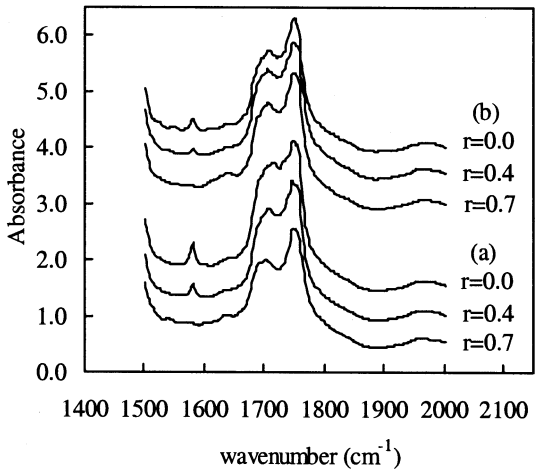

Figure 7. FT-IR spectra at three different radial positions: (a) DPS-doped fiber; (b) DPSO-doped fiber.

Beer's law, and the additive concentration profile has been determined by calculating the relative peak height for the phenyl group to that for the ester group at each radial position.

The normalized concentration profiles of DPS in the DPS-doped fibers are shown in Figure 8 for various operating conditions. The flow rate was varied between 110 and 245 g/h, which correspond to the average residence time in the annular diffusion zone of 5.5 and 2.5 min, respectively. Although attempts were made to fix the melt temperature at about 200°C, it varied between 192 and 211°C, depending on the operating conditions. The radial position of the core–cladding interface in the fiber was fixed at 0.5, which corresponds to 0.33 for the relative flow rate of the core to the cladding material. The figure indicates a significant level of molecular diffusion of DPS in the radial direction despite a short resident time of 5.5 min or smaller. Radial diffusion of the additive to such an extent is not possible if the diffusion zone is of the conventional tubular shape unless the residence time is larger by an order of magnitude (Sohn and Park, 2002).

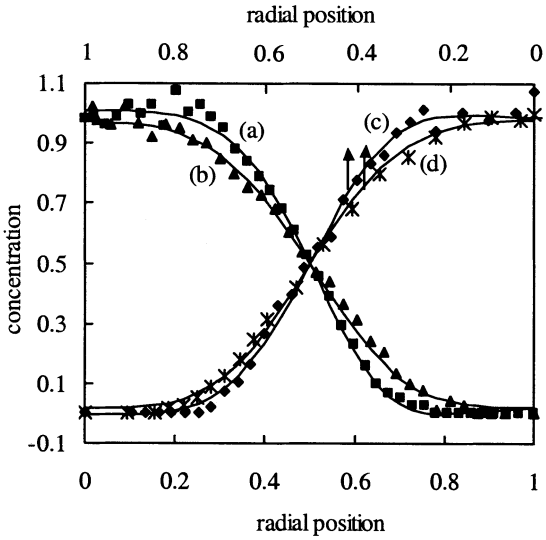

Figure 8. DPS concentration profiles in the DPS-doped GI fibers.

Solid lines are for the theoretical predictions, and symbols are experimental results at various melt temperature (T_m) and output rate. ■: $T_m = 193$°C, $Q = 153$ g/h, $D = 1.17 \times 10^{-6}$ cm^2/s; ▲: $T_m = 199$°C, $Q = 110$ g/h, $D = 1.66 \times 10^{-6}$ cm^2/s; ◆: $T_m = 209$°C, $Q = 245$ g/h, $D = 2.25 \times 10^{-6}$ cm^2/s; ∗: $T_m = 211$°C, $Q = 175$ g/h, $D = 2.42 \times 10^{-6}$ cm^2/s.

Also overlaid in Figure 8 are the theoretical predictions described by Eqs. 10 and 11 for the same operating conditions as each experiment. The diffusivity of the additive needs to be specified for the theoretical predictions. Once its diffusivity at one reference temperature is known, the diffusivity of a small molecular species in a polymer matrix at any temperature can be estimated (Ehlich and Sillescu, 1990; Heuberger and Sillescu, 1996). Thus, in calculating the predicted concentration profiles, the lowest experimental temperature (that is, 193°C) was chosen as the reference temperature, and the diffusivity of the additive at that temperature was determined by nonlinear regression to fit the experimental data to the theoretical prediction using the diffusivity as an adjustable parameter. Once the diffusivity at 193°C was determined by the curve fitting, the diffusivities at other temperatures were estimated by the free-volume theory (Vrentas and Vrentas, 1993, 1998; Vrentas et al., 1996), and the estimated values are given in the figure caption. Interested readers may refer to Sohn and Park (2002) for the detailed procedure for the estimation of the diffusivity.

In the present analysis, the additive diffusivity was assumed constant, although the diffusivity of a small molecule in a polymer matrix is an increasing function of concentration in many cases (Neogi, 1996). If the additive diffusivity depends strongly on its concentration, the concentration profile is expected to have a sharper front and a shorter tail than those described in Figures 4 to 6, because the diffusional flux of the additive is greater at higher concentrations for the same concentration gradient. However, the predicted concentration profiles match closely with the measured ones with a goodness of fit greater than 0.99. Thus, the additive diffusivity is a weak function of concentration in the range of the present investigation, justifying the constant diffusivity assumption.

Both measured and predicted concentration profiles of DPSO are shown in Figure 9. The experimental conditions were similar to those for the DPS-doped fibers, and the predicted profiles again show excellent agreement with the measured ones. The only difference we can note is that the DPSO concentration profiles are somewhat steeper than the DPS profiles at similar experimental conditions. This is due to a smaller diffusivity of DPSO than that of DPS resulting from the difference in the molecular structure and the size.

The additive concentration profiles given in Figures 8 and 9 are directly related to the refractive-index profiles through the Lorentz-Lorenz equation (Hornak, 1992)

$$n = \sqrt{\frac{1+2\phi}{1-\phi}}$$

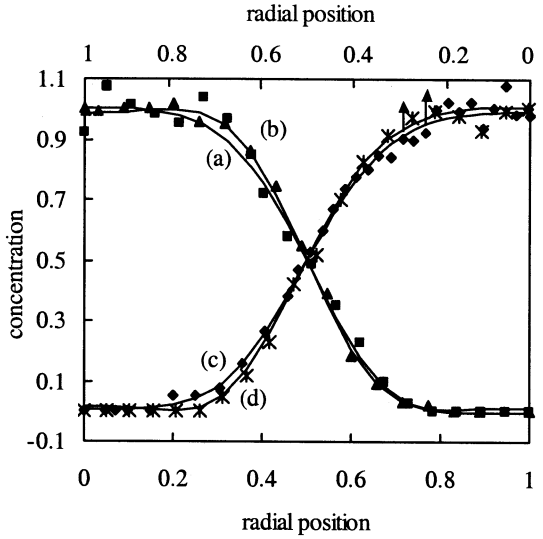

Figure 9. DPSO concentration profiles in the DPSO-doped GI fibers.

Solid lines are for the theoretical predictions, and symbols are experimental results at various melt temperature (T_m) and output rate. ■: $T_m = 193$°C, $Q = 93$ g/h, $D = 7.90\times10^{-7}$ cm^2/s; ▲: $T_m = 199$°C, $Q = 128$ g/h, $D = 9.1\times10^{-7}$ cm^2/s; ♦: $T_m = 209$°C, $Q = 151$ g/h, $D = 1.65\times10^{-6}$ cm^2/s; ∗: $T_m = 211$°C, $Q = 240$ g/h, $D = 1.88\times10^{-6}$ cm^2/s.

where

$$\phi = \frac{\Sigma_i \dfrac{(n_i^2-1)x_i}{(n_i^2+2)\rho_i}}{\Sigma_i \dfrac{x_i}{\rho_i}} \tag{13}$$

Here n is the refractive index of the mixture (that is, additive-doped PMMA); and n_i, x_i, and ρ_i are the refractive index, mass fraction, and the density of each component in the mixture, respectively. Unless the density difference between the mixture components is very large, the Lorentz-Lorenz equation indicates a near-linear relationship between the refractive index of an additive-doped material and the additive concentration. Thus, the concentration profiles given in Figures 8 and 9 closely match the normalized refractive-index profiles.

The refractive-index profile of an ideal GI-POF, which is shown in Figure 1, is often described by the power-law expression (Halley, 1987)

$$n(r) = n_1\left[1-2\Delta\left(\frac{r}{R}\right)^{\alpha}\right]^{1/2}$$

where

$$\Delta = \frac{n_1^2 - n_2^2}{2n_1^2} \tag{14}$$

Here n_1 and n_2 are the refractive indices at the center and at the outer edge of the fiber of radius R, respectively, and α is the power-law index. It is known that the bandwidth of a GI-POF shows its maximum when $\alpha = 2.0 - 2.4\Delta$. Because the value of Δ needs to be small for a wide bandwidth, the optimum value of α is close to 2, indicating that the optimum refractive index profile is of a parabolic shape. The refractive indices at the center and at the outer edge of the DPS- and DPSO-doped fibers are 1.500 and 1.492, respectively, at the prescribed concentrations (that is, $n_1 = 1.500$ and $n_2 = 1.492$), and the optimum profile that is close to the parabolic shape of Eq. 14 is achieved when the value of the dimensionless parameter k^2 in Eq. 7 is about 8.5×10^{-4} (Figure 8d). However, it should be noted that the present process utilizing the radial diffusion of the additives can result in the parabolic shape only in the central region of the fiber, and the gradually decaying tail of the sigmoidal profile is always present near the outer edge of the fiber. As will be shown in the next section, the bandwidth of the GI-POF obtained by the present process is predicted to be very high despite the nonideal profile near the edge of the fiber. When k^2 is smaller than 8.5×10^{-4} (Figures 8a, 8c, and all cases in Figure 9), the additive concentration near the center of the fiber is not yet influenced by the diffusion, so it exhibits a plateau region near the center, whereas the additive concentration at the fiber center starts to decrease when k^2 is larger than 8.5×10^{-4} (Figure 8b). Thus, in this case, the refractive index at the fiber center is smaller than 1.500 (that is, $n_1 < 1.500$).

Estimation of the Bandwidth

The bandwidth of a gradient-index optical fiber can be estimated by the Wentzel-Kramers-Brillouin (WKB) approximation once the refractive-index profile is given in an analytic form (Olshansky and Keck, 1976). However, the WKB approximation is difficult to apply if the refractive-index profile is given in such a complicated form as Eq. 10. In the present study, a numerical approach has been adopted for the bandwidth estimate following the method of ray analysis that was described in detail in our previous work (Sohn and Park, 2001).

The impulse input of a light signal spreads as it travels along the optical fiber, and this pulse spreading (that is, dispersion) limits the number of impulse inputs per unit time that can be differentiated at the outlet of the optical fiber (that is, bandwidth). There are various reasons for the dispersion in an optical fiber, including modal dispersion, material dispersion, mode coupling, and differential mode attenuation (DMA) (Garito et al., 1998; Ishigure et al., 1999; Yabre, 2000). The pulse energy injected into an optical fiber is distributed among various allowed modes. Since different modes have different group velocities, the light input spreads as it propagates along the optical fiber. The pulse spreading for this reason is called the *intermodal* or simply the *modal dispersion*. The *material dispersion* results from the finite distribution of the wavelength of the incident light and the wavelength dependence of the refractive index of the material. *Mode coupling* occurs because of the energy exchange between higher and lower modes, whereas DMA occurs because the input signal may not have uniformly distributed modes.

The material dispersion is typically smaller than the modal dispersion by orders of magnitude unless the modal disper-

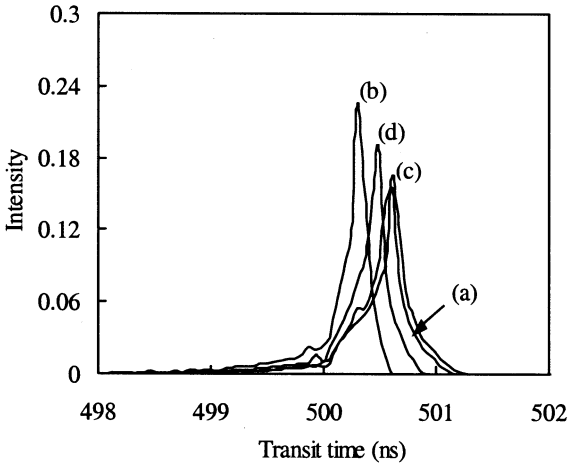

Figure 10. Impulse-response curves for the 100-m-long DPS-doped fibers with the refractive index profiles given in Figure 8 (n_1 = 1.500, n_2 = 1.492).

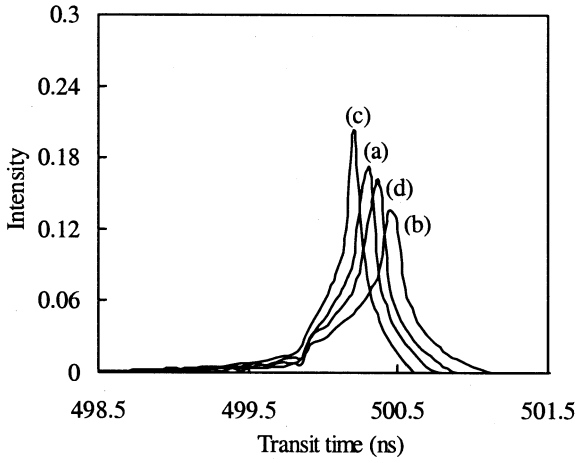

Figure 11. Impulse-response curves for the 100-m-long DPSO-doped fibers with the refractive index profiles given in Figure 9 (n_1 = 1.500, n_2 = 1.492).

sion is extremely small, as in the single-mode glass optical fibers. Mode coupling is also known to be negligible unless the fiber length is longer than 100 m. DMA, on the other hand, is known to have significant influence on the bandwidth of an optical fiber. However, it acts in a way to increase the bandwidth of POF (Ishigure et al., 1999). In the present ray analysis, only the modal dispersion was considered while neglecting all other sources of dispersion for simplicity. However, considering the fact that the material dispersion and mode coupling are negligible in the case of GI-POF for short-distance application, and that the DMA increases the bandwidth, the bandwidth estimate provided here may represent the lower limit and the actual bandwidth is expected to be larger than the predicted value.

Assuming that the input light signal has a uniform Lambertian distribution, the impulse-response curves for 100-m-long fibers with the refractive index profile shown in Figures 8 and 9 were calculated, and the results are given in Figures 10 and 11 for the DPS-doped (Figure 8) and DPSO-doped fibers (Figure 9), respectively. The refractive indices at the center and the outer edge of the fibers, which result in a numerical aperture of 0.16 for these fibers, are 1.500 and 1.492, respectively. Once the impulse-response curve is given, the bandwidth can be determined as the inverse of four times the standard deviation of the curve (that is, $1/4\sigma$) or the inverse of full-width-at-half-maximum (that is, 1/(FWHM)), and the bandwidth estimates for the eight curves given in Figures 10 and 11 are listed in Table 1.

Under the processing conditions described in the experiment section, the additive concentration profile (hence, the refractive-index profile) is essentially determined by the value of the dimensionless parameter k^2 in Eq. 7. The refractive index profile gets broader as k^2 increases and approaches closer to the ideal parabolic profile. This change in the refractive-index profile results in a narrowing of the impulse-response curve and a leftward shift toward a smaller average travel time. As Table 1 indicates, the bandwidth, estimated as the inverse of 4α, is in the 680- and 748-megabits-per-second range for the 100-m-long fiber (that is, 680–748 Mbps-100 m), whereas they are between 1,873 and 2,880 Mbps-100 m if estimated as the inverse of the FWHM. This bandwidth level well exceeds the IEEE 1394-s400 standard that requires a bandwidth of 400 Mbps-100 m for home network applications, and is substantially greater than the bandwidth of a SI-POF that is smaller than about 150 Mbps-100 m.

Summary and Conclusion

A coextrusion method using a novel die design has been introduced for the fabrication of gradient-index plastic optical fibers (GI-POF). The crux of the new die design is the presence of an inner mandrel that increases the contact area between the core and the cladding materials, thereby enhancing significantly the diffusion rate of the additive at the core–cladding interface. This new method is therefore capable of producing a high-bandwidth GI-POF at a moderately low material residence that is inconceivable with the conventional method.

A theoretical analysis indicates that the diffusion rate of the additive in the new die is much larger than that in the conventional tubular die by an order of magnitude. Experi-

Table 1. Bandwidth Estimates for the GI-POFs with the Refractive Index Profiles Described in Figures 8 and 9*

Fiber Sample	k^2	Bandwidth (Mbps-100 m)	
		$1/4\sigma$	1/(FWHM)
Figure 8a	4.80×10^{-4}	695	1,930
Figure 8b	9.46×10^{-4}	680	2,845
Figure 8c	5.76×10^{-4}	706	2,189
Figure 8d	8.67×10^{-4}	740	2,500
Figure 9a	5.33×10^{-4}	737	2,290
Figure 9b	4.46×10^{-4}	748	1,873
Figure 9c	6.85×10^{-4}	731	2,880
Figure 9d	4.91×10^{-4}	745	2,233

*Estimates were determined from the root mean square (σ) and from the FWHM of the impulse response curve.

mental results that were obtained using a PMMA along with DPS and DPSO show excellent agreement with the theoretical predictions. In addition, the bandwidth estimated by the ray analysis is shown to be well above 700 Mbps-100 m, suggesting that the new coextrusion method is a viable way to manufacture a high-bandwidth GI-POF.

Acknowledgment

The authors wish to thank Mr. Juan C. Cutie of Cyro Industries for providing PMMA samples, and Mr. Gary Scheiffele of the Engineering Research Center for Particle Science and Technology at the University of Florida for his assistance in FT-IR measurements.

Literature Cited

Ehlich, D., and H. Sillescu, "Tracer Diffusion at the Glass Transition," *Macromolecules*, **23**, 1600 (1990).
Garito, A. F., J. Wang, and R. Gao, "Effects of Random Perturbations in Plastic Optical Fibers," *Science*, **281**, 962 (1998).
Halley, P., *Fiber Optic Systems*, John Wiley, Chichester, UK (1987).
Heuberger, G., and H. Sillescu, "Size Dependence of Tracer Diffusion in Supercooled Liquids," *J. Phys. Chem.*, **100**, 15255 (1996).
Ho, B. C., J. H. Chen, W. C. Chen, Y. H. Chang, S. Y. Yang, J. J. Chen, and W. T. W. Tseng, "Gradient-Index Polymer Fibers Prepared by Extrusion," *Polym. J.*, **27**, 310 (1995).
Hornak, L. A., *Polymers for Lightwave and Integrated Optics*, Dekker, New York (1992).
Ingle, J. D., and S. R. Crouch, *Spectrochemical Analysis*, Prentice Hall, Upper Saddle River, NJ (1998).
Ishigure, T., A. Horibe, E. Nihei, and Y. Koike, "High-Bandwidth, High-Numerical Aperture Graded-Index Polymer Optical Fiber," *J. Lightwave Technol.*, **13**, 1686 (1995).
Ishigure, T., E. Nihei, and Y. Koike, "Optimum Refractive-Index Profile of the Graded-Index Polymer Optical Fiber, Toward Gigabit Data Links," *Appl. Opt.*, **35**, 2048 (1996).
Ishigure, T., M. Sato, E. Nihei, and Y. Koike, "Graded-Index Polymer Optical Fiber with High Thermal Stability of Bandwidth," *Jpn. J. Appl. Phys.*, **37**, 3986 (1998).
Ishigure, T., M. Kano, and Y. Koike, "Propagating Mode Attenuation and Coupling Characteristics of Graded-Index POF," *Proc. Int. POF Conf.*, Y. Koike, ed., ICPOF, Yokohama, Japan, p. 106 (1999).
Jakob, M., *Heat Transfer*, John Wiley, New York (1962).
Koike, Y., "High-Bandwidth Graded-Index Polymer Optical Fiber," *Polymer*, **32**, 1737 (1991).
Koike, Y., T. Ishigure, and E. Nihei, "High-Bandwidth Graded-Index Polymer Optical Fiber," *J. Lightwave Technol.*, **13**, 1475 (1995).
Liu, B. T., W. C. Chen, and J. P. Hsu, "Mathematical Modeling of a Co-extrusion Process for Preparing Gradient-Index Polymer Optical Fibers," *Polymer*, **40**, 1451 (1999a).
Liu, B. T., M. Y. Hsieh, W. C. Chen, and J. P. Hsu, "Gradient-Index Polymer Optical Fiber Preparation Through a Co-Extrusion Process," *Polym. J.*, **31**, 233 (1999b).
Michaeli, W., *Extrusion Dies for Plastics and Rubber*, 2nd ed., Hanser, New York (1991).
Neogi, P., "Transport Phenomena in Polymer Membranes," *Diffusion in Polymers*, P. Neogi, ed., Dekker, New York (1996).
Olshansky, R., and D. B. Keck, "Pulse Broadening in Graded-Index Optical Fibers," *Appl. Opt.*, **15**, 483 (1976).
Park, C. W., B. S. Lee, J. K. Walker, and W. Y. Choi, "A New Processing Method for the Fabrication of Cylindrical Objects with Radially Varying Properties," *Ind. Eng. Chem. Res.*, **39**, 79 (2000).
Sato, M., T. Ishigure, and Y. Koike, "Thermally Stable High-Bandwidth Graded-Index Polymer Optical Fiber," *J. Lightwave Technol.*, **18**, 952 (2000).
Senior, J., *Optical Fiber Communications*, Prentice Hall International, London (1985).
Siegel, R., E. M. Sparrow, and T. M. Hallman, "Steady Laminar Heat Transfer in a Circular Tube with Prescribed Wall Heat Flux," *Appl. Sci. Res.*, **A7**, 386 (1958).
Sohn, I. S., and C. W. Park, "Diffusion-Assisted Coextrusion Process for the Fabrication of Graded-Index Plastic Optical Fibers," *Ind. Eng. Chem. Res.*, **40**, 3740 (2001).
Sohn, I. S., and C. W. Park, "Preparation of Graded-Index Plastic Optical Fibers by the Diffusion-Assisted Coextrusion Process," *Ind. Eng. Chem. Res.*, **41**, 2418 (2002).
Van Duijnhoven, F. G. H., and C. W. M. Bastiaansen, "Monomers and Polymers in a Centrifugal Field: A New Method to Produce Refractive-Index Gradients in Polymers," *Appl. Opt.*, **38**, 1008 (1999).
Vrentas, J. S., and C. M. Vrentas, "Evaluation of Free-Volume Theories for Solvent Self-Diffusion in Polymer-Solvent Systems," *J. Polym. Sci.: Pt. B: Polym. Phys.*, **31**, 69 (1993).
Vrentas, J. S., and C. M. Vrentas, "Predictive Methods for Self-Diffusion and Mutual Diffusion Coefficients in Polymer-Solvent System," *Eur. Polym. J.*, **34**, 797 (1998).
Vrentas, J. S., C. M. Vrentas, and N. Faridi, "Effect of Solvent Size on Solvent Self-Diffusion in Polymer-Solvent Systems," *Macromolecules*, **29**, 3272 (1996).
Yabre, G., "Theoretical Investigation on the Dispersion of Graded-Index Polymer Optical Fibers," *J. Lightwave Technol.*, **18**, 869 (2000).

Appendix

Applying the method of separation of variables assuming $c^{(0)}(y, z) = F(y)Z(z)$, Eq. 7 is reduced to the following set of ordinary differential equations

$$\frac{6}{k^2}\frac{1}{Z}\frac{dZ}{dz} = \frac{1}{y(1-y)F}\frac{d^2F}{dy^2} = -\beta^2. \tag{A1}$$

The solution to the equation for $Z(z)$ is given as

$$Z = Ne^{-\beta^2 k^2 z/6}, \tag{A2}$$

and a series solution of the following form is sought for the equation for $F(y)$

$$F(y) = \sum_{i=0}^{\infty} B_i y^i. \tag{A3}$$

Substitution of Eq. A3 into A1 gives the following recurrence formula for the coefficients B_i of the series solution

$$B_0 = 1, \qquad B_1 = 0, \qquad B_2 = 0, \qquad B_3 = -\frac{\beta^2}{6},$$
$$B_i = \frac{\beta^2}{i(i-1)}(B_{i-4} - B_{i-3}) \quad \text{for} \quad i \geq 4. \tag{A4}$$

This recurrence formula has the following form of solution

$$B_i = \sum_{j=0}^{i} a_{ji}\beta^{2j}, \tag{A5}$$

where the a_{ji} are as follows

$$\begin{cases} a_{00} = 1 \quad a_{j0} = a_{0j} = 0 & \text{for} \quad j \geq 1 \\ a_{j1} = a_{j2} = 0 & \text{for} \quad j \geq 0 \\ a_{03} = 0 \quad a_{13} = -1/6 \quad a_{j3} = 0 & \text{for} \quad j \geq 2 \\ a_{ji} = \dfrac{1}{i(i-1)}\left[a_{(j-1)(i-4)} - a_{(j-1)(i-3)}\right] & \text{for} \quad j \geq 1 \\ & \text{and} \quad i \geq 4. \end{cases} \tag{A6}$$

Combining Eqs. A3 and A5 gives

$$F = \sum_{i=0}^{\infty} \sum_{j=0}^{i} a_{ji} \beta^{2j} y^i. \tag{A7}$$

The boundary condition (Eq. 8b) requires that the solution exists only for certain values of β defining the following characteristic equation for the eigenvalues β_n

$$\sum_{i=0}^{\infty} \sum_{j=1}^{i} i \cdot a_{ji} \cdot \beta^{2j} = 0 \tag{A8}$$

Combining Eqs. A2 and A7 then gives the solution for the concentration profile $c^{(0)}(y, z)$ as

$$c^{(0)}(y, z) = \sum_{n=1}^{\infty} N_n e^{-\beta_n^2 k^2 z/6} F_n(y, \beta_n) + C_0. \tag{A9}$$

Since Eq. 7 is a Sturm-Liouville type with weighting function $y(1-y)$, the eigenfunctions are orthogonal, satisfying the following relations

$$\int_0^1 F_n F_m y(1-y)\, dy = 0 \qquad \text{if} \qquad n \neq m \tag{A10}$$

and

$$\int_0^1 F_n F_n y(1-y)\, dy = \frac{-1}{2\beta_n} \left[F_n \frac{\partial}{\partial y} \left(\frac{\partial F_n}{\partial \beta_n} \right) \right]_{y=1} \tag{A11}$$

Thus, the coefficients N_n are determined by multiplying Eq. A9 evaluated at $z = 0$ by $F_m y(1-y)$, integrating it from 0 to 1, and applying the initial condition, Eq. 9

$$\int_0^1 c^{(0)}(y,0) F_n y(1-y)\, dy = \int_0^{Y_f} F_n y(1-y)\, dy = \int_0^1 (N_n F_n + C_0) F_n y(1-y)\, dy \tag{A12}$$

From Eq. A1

$$F_n y(1-y)\, dy = -\frac{1}{\beta_n^2} d\left(\frac{dF_n}{dy} \right) \tag{A13}$$

Thus, from Eqs. A10 through A13, the coefficient N_n is determined as

$$N_n = \frac{2}{\beta_n} \frac{\left(\frac{dF_n}{dy} \right)_{y=Y_f}}{\left[F_n \frac{\partial}{\partial y} \left(\frac{\partial F_n}{\partial \beta_n} \right) \right]_{y=1}} \tag{A14}$$

Finally, the constant C_0 is determined from the mass conservation of the additive. Because the total flux of the additive at every axial position should be same

$$\int_0^{Y_f} c^{(0)}(y,0) u_z\, dy = \int_0^1 c^{(0)}(y,\infty) u_z\, dy \tag{A15}$$

That is,

$$\int_0^{Y_f} y(1-y)\, dy = C_0 \int_0^1 y(1-y)\, dy \tag{A16}$$

Thus, the solution becomes

$$c^{(0)}(y,z) = Y_f^2 (3 - 2Y_f) + \sum_{n=1}^{\infty} N_n e^{-\beta_n^2 k^2 z/6} F_n(y, \beta_n) \tag{A17}$$

where N_n and F_n are given in Eqs. A14 and A7, respectively.

Manuscript received Dec. 9, 2002, and revision received Apr. 7, 2003.